PROCEEDINGS, 48th Workshop on Geothermal Reservoir Engineering
Stanford University, Stanford, California, February 6-8, 2023
SGP-TR-224

Development of a Discrete Fracture Network Model for Utah FORGE using Microseismic Data Collected During Stimulation of Well 16A(78)-32

Aleta Finnila[1], Branko Damjanac[2] and Robert Podgorney[3]

[1]WSP USA Inc., Redmond, WA

[2]Itasca Consulting Group, Inc., Minneapolis, MN

[3]Idaho National Laboratory, Idaho Falls, ID

aleta.finnila@wsp.com

Keywords: FORGE, DFN, 16A(78)-32, microseismic.

ABSTRACT

Previous fracture models for the Utah FORGE geothermal reservoir were developed using data from well logs and outcrop. Recent hydraulic stimulation of well 16A(78)-32 allowed for collection of high quality microseismic data which has been used to create a new fracture model based on fitting planar features to the microseismic point cloud. These planar features are interpreted to be large fractures or collections of smaller fractures sharing common orientations and locations. Fifteen hexagonal fractures are included in the new Discrete Fracture Network (DFN) model: eleven are fit from the microseismic data and four are added based on previous characterization work to provide connectivity between the fractures and the injection intervals. Previous DFN models of the site included hundreds to thousands of discrete fractures and relied on stochastic generation of features. This new simplified DFN model is created to provide an alternative fracture network having fewer discrete features and potentially captures the most significant flow pathways created by the stimulation of 16A(78)-32.

This DFN can be used for further modeling of the long-term thermal and mechanical evolution of flow paths between 16A(78)-32 and a planned production well. Our workflow for defining fractures from microseismic points is presented along with a comparison of fracture sizes and orientations between these discovered features and the fracture sets used in previous DFN models for the site.

1. INTRODUCTION

The creation of Enhanced Geothermal Systems (EGS) for power production in initially low permeability rock is expected to require the development of an extensive network of fluid pathways between injector and production wells. Hydraulic stimulation of naturally occurring fractures has been proposed as one potential mechanism to achieve this goal. As part of a US Department of Energy funded project to accelerate breakthroughs in EGS technologies, three stages of stimulation were carried out near the toe of well 16A(78)-32 in April of 2022 at the Utah FORGE site (McLennan et al., 2023). While previous fracture models of the geothermal reservoir rock relied on stochastic fracture networks conditioned by data collected from well image logs and nearby outcrops, the Microearthquake (MEQ) catalogs of the microseismic data captured during these stimulation events are used in this work to create a post-stimulation Discrete Fracture Network (DFN) model that potentially captures significant post-stimulation flow pathways in the reservoir rock. Potential planar features representing faults or fractures were identified by visual inspection while rotating the MEQ point cloud in 3D (data available from University of Utah Seismograph Stations, 2022). **Error! Reference source not found.** Additional planes were added to connect the features identified from the MEQ data based on previous fracture orientation characterization work (Finnila et al., 2021).

An important caveat to this work is that the DFN created from the workflow presented in this paper is non-unique, and is, indeed reliant on significant interpretation and interpolation by the authors. Ongoing refinements to the MEQ catalog will presumably trigger a re-evaluation of the identified features, and alternative DFN interpretations arising from this data set would be welcomed by the Utah FORGE modeling team. The DFN model described in this paper, along with other potential post-stimulation DFN models will be used for long-term simulations of production between well 16A(78)-32 and a planned production well. For computational efficiency, DFN models which capture the significant flow pathways using fewer features are preferred.

2. WORKFLOW FOR FRACTURE PLANE FITTING

While algorithms are actively being developed for automatic extraction of fracture networks from microseismic data, most of these methods rely on having event moment tensors (Yu et al., 2022) or of having the data subdivided into smaller subsets or "clusters" based on the cross-correlation of waveforms (Carmona et al., 2010; Pytharouli et al., 2011). As this level of analysis was not available at the time of this work, and the desire is to have a relatively simple resulting DFN available for modeling purposes, the choice was made to first select planar features by visual inspection of the 3D point clouds, and then to refine the selections algorithmically based on the nearby MEQ population. Details of the process are given in the following subsections.

2.1 Microseismic Point Cloud Data Preparation

Initial MEQ catalogues for the three stages of stimulation of well 16A(78)-32 are available from the Geothermal Data Repository (GDR) from University of Utah Seismograph Stations (2022). This data set includes point locations for each event in a local coordinate frame having the origin at ground level for the well, along with event times, magnitudes, estimates of location error, and other parameters that were not used for the development of the DFN. For the work presented in this paper, the point data were translated to the FORGE model global reference frame and elapsed times were calculated based on the first recorded event following the check shot. This edited data set is available from the GDR along with the well trajectory of 16A(78)-32 in the same coordinate frame (WSP Golder, 2022).

2.2 Fitting Planar Features through 16A MEQ data

The workflow used to create the DFN is described with the following steps.

For each stage:

- Visualize microseismic point cloud showing time evolution and rotate in 3D without perspective to look for linear projections that might indicate points falling on a plane. Use the colors showing elapsed time to aid in the identification of evolving slip features.

For each potential plane identified:

- Manually fit a plane to groups of points that might fall on the plane.
- Calculate distance of points to this plane.
- Filter points by distance from plane to get a subset of MEQ points – used distances in the range of 10 m to 20 m.
- Algorithmically find best-fit plane orientation to this subset of points. This workflow used the fracture pole as the eigenvector corresponding to the smallest eigenvalue from a Principal Component Analysis.
- Create a discrete fracture for the DFN where the center of the fracture is in the center of the MEQ point subset and the radius is initially set to the largest distance found between the fracture center and any MEQ point in the subset under consideration. While the fractures are treated conceptually as circular, they are generated as hexagons for easier representation in the DFN software used for this work (WSP, 2022).

Once the planar features have been identified from the MEQ data set, add a small number of connecting fractures so that all the features are connected to either well 16A(78)-32 or to another fracture in the DFN. Results of this workflow for each stage are discussed in the following subsections.

2.2.1 Stage 1

Stage 1 stimulation was conducted in the 200 ft open hole toe of well 16A(78)-32 using slickwater. The MEQ catalog for this stage included 211 events with a mean error of 141 ft. Note that the mean error for event location is much larger in Stage 1 compared with Stages 2 and 3 due to the failure of some of the recording geophones (McLennan et al., 2023). Significant seismicity was located both above and below the well. However, locations were generally significantly west of the injection zone. Four planes were fit to this data set with interpreted fractures striking north-south and having moderate dips to the west or east. Fracture radius values range from 54 m to 110 m (Figure 1).

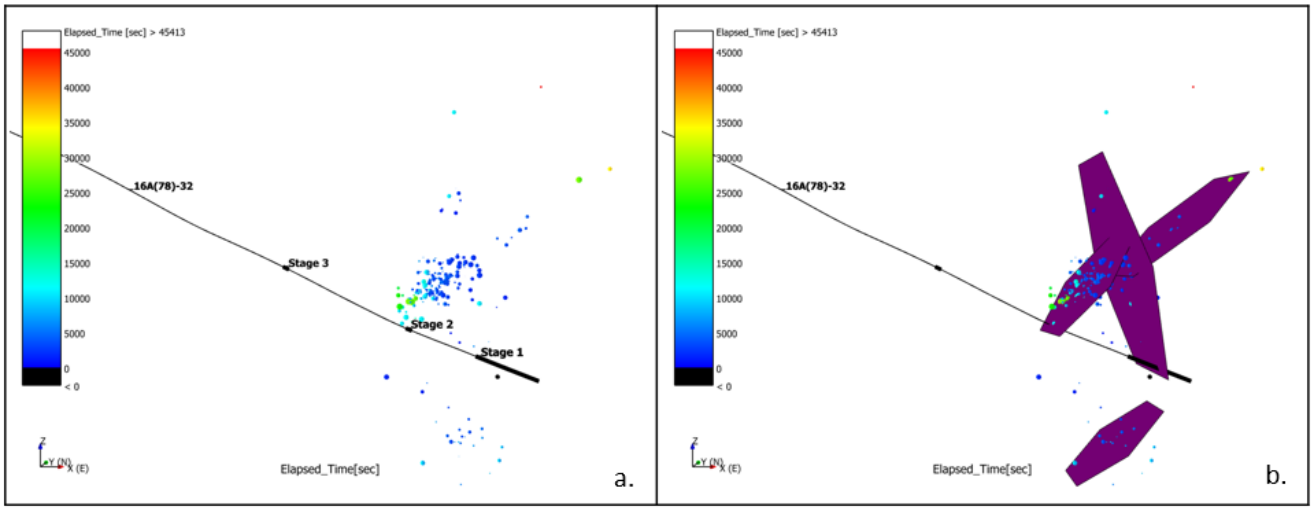

Figure 1: Side view of the preliminary MEQ catalog locations identified for the Stage 1 stimulation of well 16A(78)-32 (a); and (b) the four fracture planes identified for Stage 1. MEQ locations shown as point data with color corresponding to elapsed time from the first measured event and sizes are scaled by the calculated moment magnitude.

2.2.2 Stage 2

Stage 2 stimulation was conducted from perforation clusters in a 20-ft interval in the cased section of 16A(78)-32 using slickwater. The MEQ catalog for this stage included 948 events with a mean error of 41 ft. Stage 2 seismicity occurs primarily above the well (Figure 2). Five planes were fit to this data, all striking generally north-south and moderately dipping to the west. Assigned fracture radius values ranged from 42 m to 61 m.

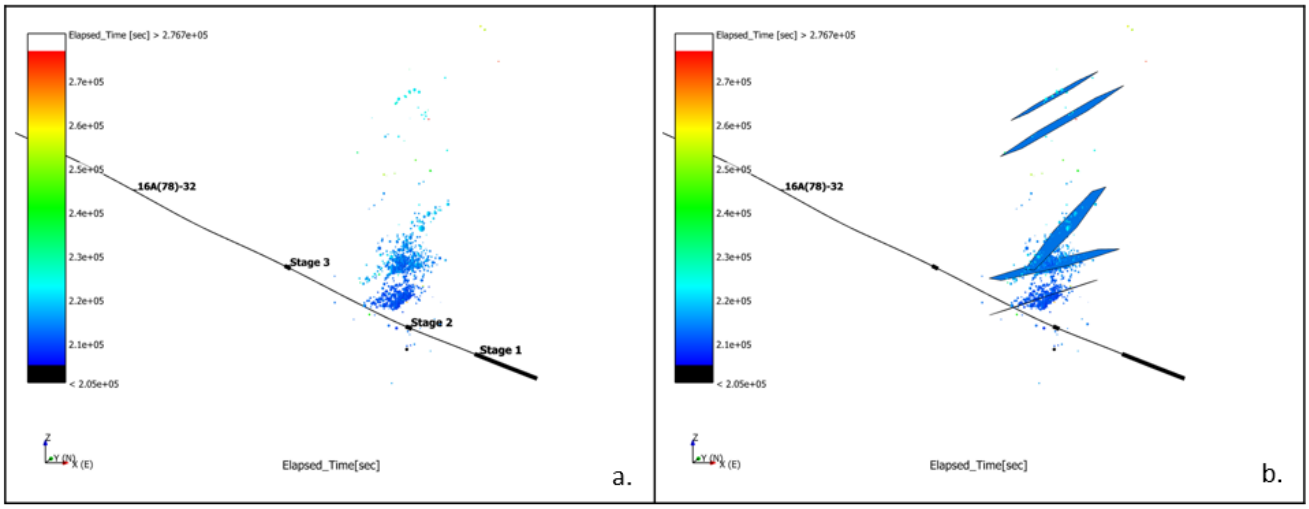

Figure 2: Side view of the preliminary MEQ catalog locations identified for the Stage 2 stimulation of well 16A(78)-32 (a); and (b) the five fracture planes identified for Stage 2. MEQ locations shown as point data with color corresponding to elapsed time from the first measured event and sizes are scaled by the calculated moment magnitude.

2.2.3 Stage 3

Stage 3 stimulation was conducted from perforation clusters in a 20-ft interval in the cased section of 16A(78)-32 using a crosslinked gel. The MEQ catalog for this stage included 1432 events with a mean error of 56 ft. Most of the Stage 3 microseismicity locations are consistent with the extension of a single large hydraulic fracture or possibly a number of smaller natural fractures connected by a new hydraulic fracture. The stimulation extent is approximately 150 m above and 50 m below the well with the lateral extent being somewhat greater than the vertical extent. The MEQ point cloud was roughly fit using two vertical planes, one striking close to the orientation of the expected maximum principal stress at N24E and another to the north of the well striking north-south (Figure 3). The larger fracture was given a radius of 149 m and the smaller fracture to the north was assigned a radius of 74 m.

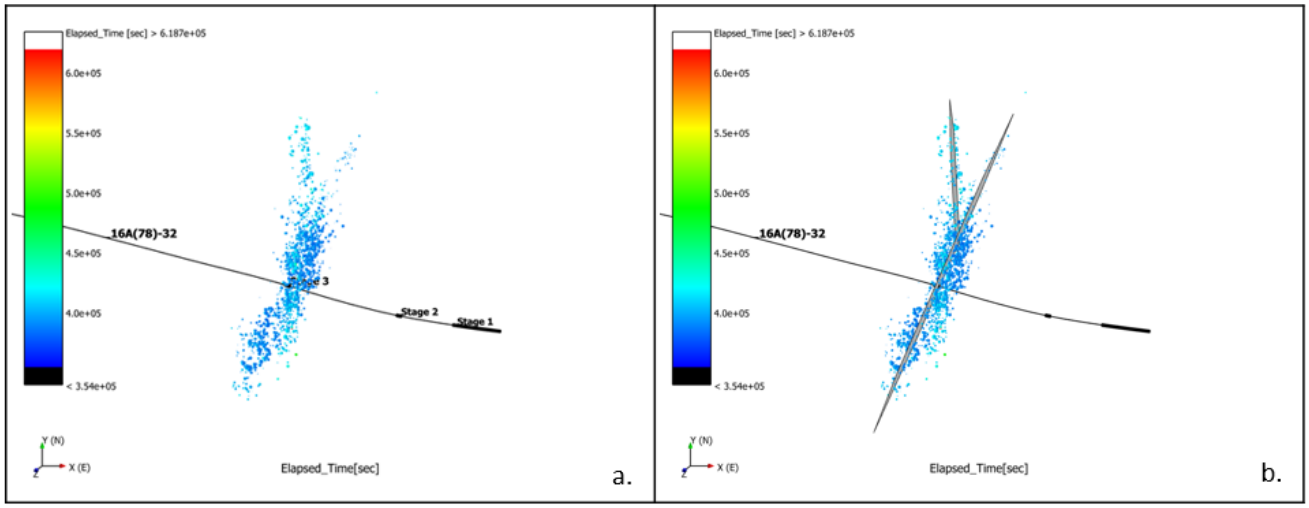

Figure 3: Top-down view of the preliminary MEQ catalog locations identified for the Stage 3 stimulation of well 16A(78)-32 (a); and (b) the two fracture planes identified for Stage 3. MEQ locations shown as point data with color corresponding to elapsed time from the first measured event and sizes are scaled by the calculated moment magnitude.

2.3 Add Connecting Planes to DFN

Given that the driving motivation for creating this DFN is to use it for modeling flow between well 16A(78)-32 and a future producer well, it is important for the fractures to be connected both to the well and each other. This was accomplished by increasing the radius of some of the planar features identified from the MEQ data and by adding some extra planes that are consistent with the orientations of the natural fractures identified from image logs of the reservoir rock. Figure 4 shows the four added fracture planes: the bottom two were added to connect the plane identified from microseismicity located below the well; one smaller one was added to better connect the Stage 2 fractures with the injection zone; a fourth was added to connect the upper top two fitted planes for Stage 2.

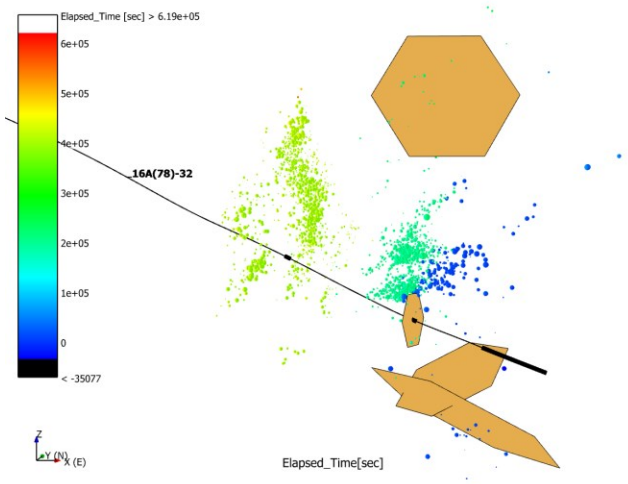

Figure 4: Side view of four extra fracture planes added to the fit planes in the fracture model in order to create a connected DFN.

The specification of these connecting fractures is somewhat arbitrary. Their orientations were selected based both on similarity to previously identified features from image log data, the presence of small numbers of microseismic events, and/or the efficacy of connecting with features previously identified. Significant flow pathways can be present without triggering detectable seismic events during hydraulic stimulation (see Wei et al., 2022, for a review of slip mechanisms). These may be due the presence of open features that are permeable without new failures occurring, features able to slip aseismically due to material properties, or opening (i.e. with small in-situ shear stress) or slipping features that trigger ruptures, however, the signal is too small to detect.

3. DISCUSSION OF THE MICROSEISMIC DFN

The final 15-fracture DFN is shown in Figure 5 and is available for download from the GDR (WSP Golder, 2022). Note that there are two fit fractures for Stage 3 where the smaller fracture is mostly obscured in this view; the vertical line seen near 16A on the large grey fracture shows the intersection between the two.

The orientations of the planar features identified using the MEQ data are shown in Figure 6 along with the orientations of the added connecting fractures and the mean poles of the four natural fracture sets identified from image logs (Finnila, 2021). The features identified from microseismic data for Stage 1 primarily seem to be members of the previously identified south striking, moderately dipping west fracture set. This set was predicted to be the most numerous of the four identified natural fracture sets, representing approximately 36% of the fracture population. One additional feature aligned with the north striking steeply dipping east set. Features identified from Stage 2 are similar to those in Stage 1 with all five aligning with the south striking, moderately dipping west fracture set. The two Stage 3 features include one in the expected orientation for a hydraulic fracture which is consistent with the south-southwest striking vertical set and the other seems to be a member of the north striking steeply dipping east set. While no features consistent with being members of the fourth fracture set were identified from the microseismic data, east striking steeply dipping south, one connecting fracture in that orientation was included. DFN fracture orientations are provided in the GDR data set using two equivalent conventions: fracture pole trend and plunge, and fracture plane strike and dip.

The fracture sizes included in the DFN have radius values ranging between 25 m and 149 m which are large but still consistent with the fracture population previously characterized with a truncated power law distribution having a power law exponent of 3.2 and a minimum fracture radius of 0.63 m (Finnila, 2021). Previous stochastic DFNs for the site included fractures having radius values between 10 m and 150 m where 5% of those fractures had radius values larger than 25 m. Given the motivation for developing this new DFN model is to provide a small number of fractures representing significant fluid pathways for future simulation work, choosing a single larger feature instead of a collection of smaller, similarly oriented features was preferred. Each individual fracture included in the DFN may well represent sets of smaller, connected fractures.

Rough estimates of fracture aperture, permeability and compressibility are provided in the GDR DFN data set, however, there was no new work performed in this study to refine these values. The post-stimulation fracture apertures for the DFN were assigned to the constant

value 0.2 mm based on the simulation work performed by Xing et al. (2022). Actual fracture apertures values are not well constrained and are expected to be dependent on fracture size, roughness, compressibility, infill material, among other parameters. Using this single aperture value, fracture permeability was calculated using the parallel-plate cubic law to be $3x10^{-9}$ m^2. Fracture compressibility was assigned as $5x10^{-6}$ 1/kPa based on estimates of whole rock compressibility of $3.3 x10^{-8}$ 1/kPa and a fracture porosity of 0.66% (see Finnila et al., 2021, for further discussion of estimating fracture compressibility in a DFN).

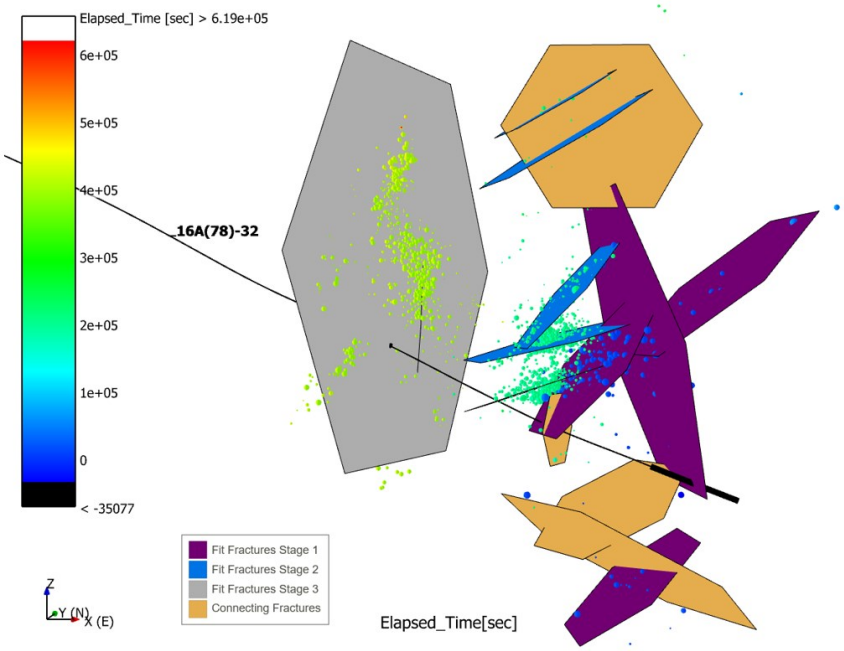

Figure 5: Side view of the 15 fracture planes included in the updated reference DFN model based on an interpretation of the preliminary MEQ catalog from the stimulation of well 16A(78)-32. MEQ locations are shown as point data with color corresponding to elapsed time from the first measured event and sizes are scaled by the calculated moment magnitude.

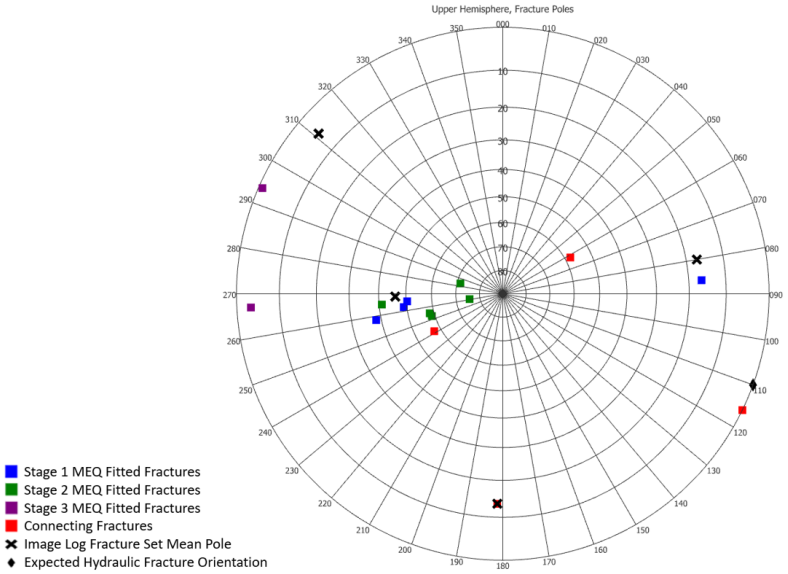

Figure 6: Upper hemisphere stereonet of the 15 fractures included in the DFN generated using MEQ catalog data (squares) and the mean fracture poles of the four previously identified natural fracture sets (crosses). The expected orientation of a hydraulic fracture due to the site principal stresses is also shown (diamond).

4. CONCLUSION

The workflow used to create a 15-fracture DFN based on the MEQ catalogs prepared from the stimulation of well 16A(78)-32 at Utah FORGE has been presented in this paper. This DFN can be used to for simulations of post-stimulation flow paths between potential well 16A(78)-32 and potential producer wells and is available from the GDR (WSP Golder, 2022). Other DFN interpretations are possible using the same data set or future enhancements to the MEQ catalogs and other researchers are encouraged to develop alternative models for use in predictive modeling at the Utah FORGE site.

ACKNOWLEDGEMENTS

Funding for this work was provided by the U.S. DOE under grant DE-EE0007080 "Enhanced Geothermal System Concept Testing and Development at the Milford City, Utah FORGE Site". We thank the many stakeholders who are supporting this project, including U.S. DOE Geothermal Technologies Office, Smithfield (Murphy Brown LLC), Utah School and Institutional Trust Lands Administration, and Beaver County as well as the Utah Governor's Office of Energy Development.

REFERENCES

Carmona, E., J. Almendros, J. A. Peña, and J. M. Ibáñez (2010), Characterization of fracture systems using precise array locations of earthquake multiplets: An example at Deception Island volcano, Antarctica, J. Geophys. Res., 115, B06309.

Finnila, A.: Estimation of Fracture Size for a Discrete Fracture Network Model of the Utah FORGE Geothermal Reservoir using Forward Modeling of Fracture-Borehole Intersections. Paper presented at the 55th U.S. Rock Mechanics/Geomechanics Symposium, physical event cancelled, June 2021. Originally accepted for the 3rd International Discrete Fracture Network Engineering Conference. DFNE 21-2329 (2021).

Finnila, A., Doe, T., Podgorney, R., Damjanac, B., and Xing, P.: Revisions to the Discrete Fracture Network Model at Utah FORGE Site, GRC Transactions, Vol 45, (2021).

McLennan, J., England, K., Rose, P., Moore, J., and Barker, B. Stimulation of a High-Temperature Granitic Reservoir at the Utah FORGE Site, Proceedings, SPE Hydraulic Fracturing Technology Conference and Exhibition, The Woodlands, Texas (2023).

Pytharouli, S. and Lunn, R. and Shipton, Z. and Kirkpatrick, J. and do Nascimento, A.: Microseismicity illuminates open fractures in the shallow crust. Geophysical Research Letters, 38, (2011), L02402.

University of Utah Seismograph Stations: Seismic Data from the Well 16A(78)-32 Stimulation April, 2022 [data set]. Retrieved from https://dx.doi.org/10.15121/1879450, (2022).

Wei W., Dazhao L., and Elsworth, D.: Fluid injection-induced fault slip during unconventional energy development: A review, Energy Reviews, Volume 1, Issue 2, (2022), 100007.

WSP: FracMan® Reservoir Edition, version 8.1 Discrete Fracture Network Simulator, (2022).

WSP Golder: Utah FORGE Well 16A(78)-32 Stimulation DFN Fracture Plane Evaluation and Data [data set]. Retrieved from https://dx.doi.org/10.15121/1901784, (2022).

Xing, P., Damjanac, B., Radakovic-Guzina, Z., Maurilio, T., Finnila, A., Podgorney, R., Moore J., and McLennan, J.: Numerical Simulation of Injection Tests at Utah FORGE Site, GRC Transactions, Vol. 46, (2022).

Yu J., Joo Y. and Kim B-Y.: A multimodel fitting algorithm for extracting a fracture network from microseismic data. Front. Earth Sci. 10:961277, (2022).